NATIONAL TECHNICAL UNIVERSITY OF ATHENS

SCHOOL OF APPLIED MATHEMATICAL AND PHYSICAL SCIENCES

INTERNSHIP ASSIGNMENT

Study of recursive computation of scattering amplitudes and applications to LO phenomenology

Name:
Georgia ZACHOU

Supervisors:
C. PAPADOPOULOS
G. BEVILACQUA

Professor:
N. MAVROMATOS

Contents

1   Introduction

The current work serves a personal report, presenting the two main projects of my 2-month internship. The theoretical work will also be included since it was essential training before undertaking the main projects. The purpose is to provide an overview of the subjects we became familiar with and the knowledge gained throughout this process. To begin with, we will shortly present the basic concepts of QFT and focus primarily on Feynman rules by illustrating analytically calculated examples for QED and QCD. The first project is a computational exercise for symbolic calculations in the Standard Model Effective Field Theory (SMEFT)[1]. As a part of my training, I developed a python library with tools that contribute in computing the currents based on the operators O_{uG}, O_{uH} and O_{HG}. Our interest is concentrated mainly to those operators since they are play an extraordinary role in processes with top quark production at the LHC (such as ttH). These equations could be used for recursive computations at a tree-level in the framework of SMEFT. The second project aims at gaining some basic experience with phenomenological studies using LHC data. Specifically, we consider an extension of the standard model that introduces a Z' singlet mediator, which interacts only with top-antitop pairs. This model is knwon as top-philic Z' model in the literature[2]. I have implemented the model in the HELAC-PHEGAS interface and performed a phenomenological analysis considering the process $pp \to t\bar{t}t\bar{t}$ at leading-order(LO) perturbation theory. The internship has provided not only a better understanding of the theoretical concepts through analytical calculations practice, but also improved my skills in utilizing programming tools and interfaces, such as Python and HELAC-PHEGAS.

2   Field theory

2.1   QED

Quantum Electrodynamics is the quantum field theory that best describes the electromagnetic interactions. The propagator of the force in this case is a photon (massless of spin-1). QED consists of the Maxwell's and Dirac equations determined by relativistic invariance. If we take the Dirac Lagrangian, then add the Maxwell term and consider a covariant derivative of the form:

$$\partial_\mu \to D_\mu = \partial_\mu + iqA_\mu \tag{2.1.1}$$

The final form of the QED Lagrangian through this transformation is:

$$\mathcal{L}_{Dirac} = \bar{\psi}(i\partial\!\!\!/ - m)\psi \xrightarrow{+L_{Maxwell}} \mathcal{L}_{QED} = \bar{\psi}(i\partial\!\!\!/ - m)\psi - \underbrace{\frac{1}{4}F^{\mu\nu}F_{\mu\nu}}_{L_{Maxwell}} - \underbrace{q\bar{\psi}\gamma^\mu\psi A_\mu}_{\text{interaction term}} \tag{2.1.2}$$

where $F^{\mu\nu} = \partial_\mu A_\nu - \partial_\nu A_\mu$. This Lagrangian is invariant under local U(1) transformations:

$$\psi(x) \to e^{-i\alpha(x)}\psi(x) \;, \quad A_\mu(x) \to A_\mu(x) - \frac{1}{q}\partial_\mu\alpha(x) \tag{2.1.3}$$

The Feynman rules that constitute the QED are shown in 2. We are going to use them in LO-cross sections calculation examples in this assignment:

Figure 1: Feynman Rules for QED

2.2 QCD

Quantum Chromodynamics is a non-Abelian gauge theory that describes strong interactions. The mediators in this theory are gluons. The SU(3) local phase transformation is:

$$\psi(x) \to \psi'(x) = e^{ig\alpha^a(x)t^a}\psi(x) \tag{2.2.1}$$

The matrices t_a obey the commutation rule: $[t_a, t_b] = if_{abc}t_c$ and they are the 8 generators of the SU(3) Lie algebra. In this case, to maintain the invariance of the Lagrangian under 2.2.1, the covariant derivative is replaced:

$$\partial_\mu \to D_\mu = \partial_\mu - igA_\mu^a t_a \tag{2.2.2}$$

Where $\alpha = 1, ..., 8$ and each field A_μ^a is the gluon field strength. The final QCD Lagrangian is given by:

$$\mathcal{L}_{QCD} = \sum_i \bar{\psi}_i(i\slashed{D} - m_i)\psi_i - \frac{1}{4}F_{\mu\nu}{}^a F^{a\mu\nu} \tag{2.2.3}$$

Because of the non-abelian character of this theory, gluon's self interaction must be included in the Feynman rules. Specifically, we may have a 3-gluon or a 4-gluon vertex.
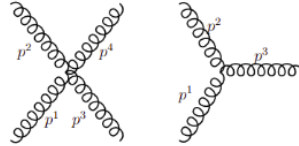

Figure 2: Gluon self-interaction

It is essential that we know how to predict the number of Feynman diagrams using the Feynman rules in order to compare the analytical results against HELAC interface during the simulations.

2.3 QCD color decomposition- Graphical approach

Let us explain the color decomposition process using a more graphical approach[3]. For each set of operators, we can have graphical representation.

There are $N_c = 3$ colors in QCD which define the identity of quarks and gluons. Quarks and antiquarks use a lower index q_i where $i \in 1, 2, 3$ and gluons which are the mediators of the strong force are denoted g^α where $\alpha \in 1, 2, ..., 8$. The general rules for color decomposition are shown below:

-
$$q\bar{q}g = \quad a \ = T_{ij}^{\alpha} = \frac{1}{\sqrt{2}}\tau_{ij}^{\alpha}$$

-
$$q\bar{q} = \quad = \delta_{ij}$$

-
$$ggg = \quad b \ = if^{abc}$$

The above operators compose the $SU(3)$ group algebra. Some significant properties are found below, and will be used a lot in the calculations:

- $[T^a, T^b] = if^{abc}T^c$

- $Tr[T^a T^b] = T_R \delta^{ab}$

- Fierz identity:

$$T_{ij}^{\alpha}T_{kl}^{\alpha} = T_R\left(\delta_{il}\delta_{kj} - \frac{1}{N_c}\delta_{il}\delta_{kj}\right)$$

$$\Rightarrow \quad = T_R\left(\quad -\frac{1}{N_c} \quad \right)$$

-
$$if^{abc} = \frac{1}{T_R}Tr[T^a T^b T^c - T^c T^b T^a]$$

$$\Rightarrow \quad = \quad - \quad$$

At this point, we will provide a detailed example to illustrate the color decomposition technique. We will prove, using the graphic and algebraic representation, the relation:

$$[f^{abc}L_1](\tau^{\alpha_1})_{i_1 j_1}(\tau^{\alpha_2})_{i_2 j_2}(\tau^{\alpha_3})_{i_3 j_3} = \left(-\frac{i}{\sqrt{2}}\right)\delta_{i_1 j_2}\delta_{i_2 j_3}\delta_{i_3 j_1} + \left(\frac{i}{\sqrt{2}}\right)\delta_{i_3 j_2}\delta_{i_2 j_1}\delta_{i_1 j_3} \qquad (2.3.1)$$

Starting with the first part:

$$1^{st} \text{ part} = [f^{abc}L_1]\,(\tau^{\alpha_1})_{i_1 j_1}(\tau^{\alpha_2})_{i_2 j_2}(\tau^{\alpha_3})_{i_3 j_3}$$

$$= \frac{1}{2i\sqrt{2}} tr[\tau^{\alpha_1}\tau^{\alpha_2}\tau^{\alpha_3} - \tau^{\alpha_3}\tau^{\alpha_2}\tau^{\alpha_1}](\tau^{\alpha_1})_{i_1 j_1}(\tau^{\alpha_2})_{i_2 j_2}(\tau^{\alpha_3})_{i_3 j_3}L_1$$

 (2.3.2)

$$\overset{\text{Fierz Id. for a, b, c}}{=} \left(-\frac{i}{\sqrt{2}}\right)\delta_{i_1 j_2}\delta_{i_2 j_3}\delta_{i_3 j_1} + \left(\frac{i}{\sqrt{2}}\right)\delta_{i_3 j_2}\delta_{i_2 j_1}\delta_{i_1 j_3} = 2^{nd} \text{ part}$$

The Fierz identity was performed for each of the a, b, c gluons giving 2 extra terms every time we contract with each $(\tau^\alpha)_{ij}$ operator. In the end, though, we are left with only two final results.

2.4   Introduction to SMEFT

In this chapter, we will discuss the Standard Model Effective Field Theory and explore the reasons why it is an important consideration in phenomenology. We will outline the fundamentals of SMEFT[4] to ensure that the results of our study are clear and comprehensible.

Since the discovery of the Higgs boson at the LHC a decade ago, no clear evidence of new physics has emerged at the specific TeV scale at which the LHC operates (with an energy limit of 13.6 TeV). Today, many scientists are convinced that physics beyond the Standard Model possibly exists at higher energy scales than those currently accessible by the LHC. Theoretical evidence continues to motivate researchers to explore these larger scales in the search for new physics.

Let us begin by pointing out the issues in the current field theory.

Assuming that new physics is "heavy" and therefore detectable only at higher energy scales, scientists have explored how the Standard Model would be modified by the presence of this heavier physics making various corrections in the standard model Lagrangian. Using the SMEFT framework, it has been proved that the SMEFT Lagrangian at its low energy limit actually matches the measurements we already have based on the standard model.[1]

Assume $SU(3) \times SU(2) \times U(1)$ gauge theory with no more light particles and that Higgs boson is a part of $SU(2)$ doublet. In this case, only SM particles exist, however new interactions appear. The SMEFT Lagrangian is an expansion of the standard model Lagrangian, which at the same time represents the lower energy term, with some additional terms:

$$\mathcal{L} = \underbrace{\mathcal{L}_{SM}}_{d=4} + \sum_i C_i^{(6)}\frac{\mathcal{O}_i^{d=6}}{\Lambda^2} + \sum_i C_i^{(8)}\frac{\mathcal{O}_i^{d=8}}{\Lambda^4} + ... \tag{2.4.1}$$

The constants $C_{,i}^{(6)}, C_i^{(8)}...$ may be many and they are called Wilson coefficients. Correspondingly, there

are the EFT operators $\mathcal{O}_i^{d=6}, \mathcal{O}_i^{d=8}$, and the parameter Λ represents the energy scale, whose power depends on the dimension of the operator.

In this assignment we will be dealing only with the dimension-6 operator. The dimension-6 operators $\mathcal{O}_i^{d=6}$ in the Warsaw basis are listed in figure 3. They are categorized into those that interact with bosonic fields and remain invariant under $SU(3)$ transformations, and those that interact with fermionic fields, which can be further classified based on their transformation properties under $SU(3)$ variations.

Although it would be interesting to study each of them individually, our primary focus is on three specific ones, the O_{uG}, O_{uH} and O_{HG}.

In another classification based on the primary types of physical observables or processes that constrain these operators, the first two are EWPO (electroweak precision observables) operators, and the last one is bosonic. This means that the first two operators could affect electroweak processes, potentially causing deviations in measurements, while the last one would influence measurements involving bosonic fields.

Figure 3: Dimension-6 operators in the Warsaw basis. The grey cells indicate operators that break flavour $SU(3)$ explicitly.[1]

$$
\begin{aligned}
\text{EWPO:} \quad & \mathcal{O}_{HWB}, \mathcal{O}_{HD}, \mathcal{O}_{ll}, \mathcal{O}_{Hl}^{(3)}, \mathcal{O}_{Hl}^{(1)}, \mathcal{O}_{He}, \mathcal{O}_{Hq}^{(3)}, \mathcal{O}_{Hq}^{(1)}, \mathcal{O}_{Hd}, \mathcal{O}_{Hu}, \\
\text{Bosonic:} \quad & \mathcal{O}_{H\Box}, \mathcal{O}_{HG}, \mathcal{O}_{HW}, \mathcal{O}_{HB}, \mathcal{O}_W, \mathcal{O}_G, \\
\text{Yukawa:} \quad & \mathcal{O}_{\tau H}, \mathcal{O}_{\mu H}, \mathcal{O}_{bH}, \mathcal{O}_{tH}. \quad\quad\quad (2.8)
\end{aligned}
$$

Figure 4: Classification of the operators based on the impacts they will show in different measurements and processes.[1]

In our research we will be dealing with the $t\bar{t}H$ interaction[5]. The top quark and the Higgs boson are the two heaviest elements in the SM until today. As a result, using SMEFT, this interaction is expected to reveal evidence of beyond the SM physics. The SMEFT introduces additional correction terms into the Lagrangian at the Next-to-Leading Order (NLO) approximation. This means that, for certain sets of particles, such as in this case, there will be more interactions, including off-shell ones, beyond those typically observed in the Standard Model.

As previously mentioned, the operators under investigation are O_{uG}, O_{uH} and O_{HG}. Examples of effective vertices generated by these operators are provided below:
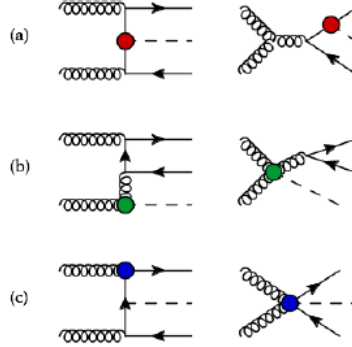
Figure 5: Example diagrams for $t\bar{t}H$ production. (a)$O_{t\phi}$, (a)$O_{\phi G}$ and (a)O_{tG}

SMEFT predictions in general are important for several reasons. To understand their contribution in physics, we will provide a similar example.

In 1930, Fermi predicted the $\mu^- \nu_\mu \to e^- \bar{\nu}_e$ interaction. However, he introduced the coupling. However, at that time, Fermi did not know that this interaction was related to the W-boson exchange, as later described by the modern Standard Model. Similarly, SMEFT operates on the principle of using effective interactions to describe possible new physics. By introducing NLO terms that are fitted to existing SM measurements, SMEFT allows us to explore additional interactions that might occur, even if their mechanisms are not yet fully understood.

In order to start our investigation, in Section 4, we introduce a Python library designed to symbolically calculate the output currents, scalars, and vectors based on the process and operator involved in the interactions. In this way, we will be able to implement the symbolically generated currents in HELAC-PHEGAS[6] simulation tool, make the fitting according to standard model and eventually explore the SMEFT interactions.

3   Examples of Analytical calculations

By applying Feynman rules and trace techniques, one can calculate scattering amplitudes for the QED and QCD processes. In the following, we will present the analytical calculations; however, such calculations are automated using the HELAC interface, which we will discuss further in the next section.

3.1   QED: Bhabha scattering

Using M.D. Schwartz's notation, calculations have been conducted to
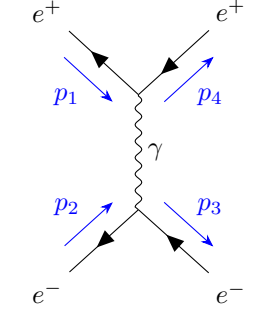
(a) scattering: t-channel
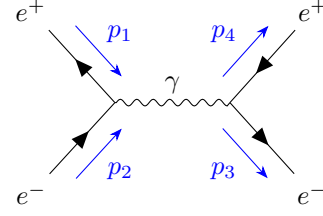
(b) annihilation: s-channel

In order to find the S-matrix element for the Bhabha scattering, we need to sum over all the matrix elements of all possible Feynman diagrams of the process. In our case we have a t-channel and an s-channel, so the sum will become:

$$\mathcal{M} = \mathcal{M}_t + \mathcal{M}_s \Rightarrow$$
$$\langle|\mathcal{M}|^2\rangle = \frac{1}{4}\sum_{s,s'}\left(|\mathcal{M}_t|^2 + |\mathcal{M}_s|^2 + \mathcal{M}_s\bar{\mathcal{M}}_t + \mathcal{M}_t\bar{\mathcal{M}}_s\right) \tag{3.1.1}$$

Following the appropriate convention for the momenta directions, the matrix elements for both t and s-channels are presented below:

$$\mathcal{M}_t = \bar{u}(p_3)(-ie\gamma^\mu)u(p_2)\left(\frac{-ig_{\mu\nu}}{q^2}\right)\bar{v}(p_4)(-ie\gamma^\nu)v(p_1)$$
$$\mathcal{M}_t = -\frac{e^2}{t}[\bar{u}(p_3)\gamma^\mu u(p_2)][\bar{v}(p_4)\gamma_\mu v(p_1)] \tag{3.1.2}$$

$$\mathcal{M}_s = \bar{u}(p_2)(-ie\gamma^\mu)v(p_1)\left(\frac{-ig_{\mu\nu}}{q^2}\right)\bar{v}(p_4)(-ie\gamma^\nu)u(p_3)$$
$$\mathcal{M}_s = -\frac{e^2}{s}[\bar{u}(p_2)\gamma^\mu v(p_1)][\bar{v}(p_4)\gamma_\mu u(p_3)] \tag{3.1.3}$$

We will now calculate the sum over all spins of the matrix element squared:

$$\sum_{s,s'}|\mathcal{M}_t|^2 = \frac{e^4}{q^4}\left([\bar{u}(p_3)\gamma^\mu u(p_2)][\bar{v}(p_4)\gamma_\mu v(p_1)]\right)\left([\bar{u}(p_3)\gamma^\mu u(p_2)][\bar{v}(p_4)\gamma_\mu v(p_1)]\right)^\dagger$$

$$= \frac{e^4}{q^4}\left([\bar{u}(p_3)\gamma^\mu u(p_2)][\bar{v}(p_4)\gamma_\mu v(p_1)]\right)\left([\bar{v}(p_1)\gamma_\nu v(p_4)][u(p_2)\gamma^\nu \bar{u}(p_3)]\right)$$

$$= \frac{e^4}{q^4}[\bar{u}(p_3)\gamma^\mu u(p_2)][u(p_2)\gamma^\nu \bar{u}(p_3)][\bar{v}(p_4)\gamma_\mu v(p_1)][\bar{v}(p_1)\gamma_\nu v(p_4)]$$

$$= \frac{e^4}{q^4}[\bar{u}_a(p_3)\gamma^\mu_{ab} u_b(p_2)u_c(p_2)\gamma^\nu_{cd}\bar{u}_d(p_3)][\bar{v}^i(p_4)\gamma^{ij}_\mu v^j(p_1)\bar{v}^k(p_1)\gamma^{kl}_\nu v^l(p_4)]$$

At this point, one can notice that for the fermions the trace can be written as:

$$u_i(p)\bar{u}_j(p) = (\not{p} + m) \tag{3.1.4}$$

and correspondingly for the antifermions:

$$v_i(p)\bar{v}_j(p) = (\slashed{p} - m) \tag{3.1.5}$$

Where i,j the spin indices. Using those two relations we continue the calculation:

$$\sum_{s,s'} |\mathcal{M}_t|^2 = \frac{e^4}{t^2}[\bar{u}_a(p_3)\gamma^\mu_{ab}(\slashed{p}_2 + m)\gamma^\nu_{cd}\bar{u}_d(p_3)][\bar{v}^i(p_4)\gamma^{ij}_\mu(\slashed{p}_1 - m)\gamma^{kl}_\nu v^l(p_4)]$$

$$= \frac{e^4}{t^2}tr[(\slashed{p}_3 + m)\gamma^\mu(\slashed{p}_2 + m)\gamma^\nu)]tr[(\slashed{p}_4 - m)\gamma_\mu(\slashed{p}_1 - m)\gamma_\nu]$$

$$= \frac{e^4}{t^2}\left(tr[\slashed{p}_3\gamma^\mu\slashed{p}_2\gamma^\nu] + m^2 tr[\gamma^\mu\gamma^\nu)]\right)\left(tr[\slashed{p}_4\gamma_\mu\slashed{p}_1\gamma_\nu] - m^2 tr[\gamma_\mu\gamma_\nu)]\right)$$

$$= \frac{e^4}{t^2}\left(p_{3\rho}p_{2\sigma}tr[\gamma^\rho\gamma^\mu\gamma^\sigma\gamma^\nu] + 4m^2 g^{\mu\nu}\right)\left(p_{4\rho}p_{1\sigma}tr[\gamma_\rho\gamma_\mu\gamma_\sigma\gamma_\nu] - 4m^2 g_{\mu\nu}\right)$$

$$= \frac{e^4}{t^2}\left(p_{3\rho}p_{2\sigma}(g^{\rho\mu}g^{\sigma\nu} - g^{\rho\sigma}g^{\mu\nu} + g^{\rho\nu}g^{\mu\sigma}) + 4m^2 g^{\mu\nu}\right)\left(p_{4\rho}p_{1\sigma}(g_{\rho\mu}g_{\sigma\nu} - g_{\rho\sigma}g_{\mu\nu} + g_{\rho\nu}g_{\mu\sigma}) - 4m^2 g_{\mu\nu}\right)$$

$$= 16\frac{e^4}{t^2}(\rho^\mu_3 \cdot \rho^\nu_2 - g^{\mu\nu}(\rho_3 \cdot \rho_2) + \rho^\nu_3 \cdot \rho^\mu_2 - m^2 g^{\mu\nu})(\rho_{4\mu} \cdot \rho_{1\nu} - g_{\mu\nu}(\rho_4 \cdot \rho_1) + \rho_{4\nu} \cdot \rho_{1\mu} - m^2 g_{\mu\nu})$$

$$= 16\frac{e^4}{t^2}(\rho^\mu_3 \cdot \rho^\nu_2 \cdot \rho_{4\mu} \cdot \rho_{1\nu} - g_{\mu\nu}\rho^\mu_3 \cdot \rho^\nu_2(\rho_4 \cdot \rho_1) + \rho^\mu_3 \cdot \rho^\nu_2 \cdot \rho_{4\nu} \cdot \rho_{1\mu} - \rho^\mu_3 \cdot \rho^\nu_2 m^2 g_{\mu\nu} +$$

$$- g^{\mu\nu}(\rho_3 \cdot \rho_2)\rho_{4\mu} \cdot \rho_{1\nu} + g^{\mu\nu}(\rho_3 \cdot \rho_2)g_{\mu\nu}(\rho_4 \cdot \rho_1) - g^{\mu\nu}(\rho_3 \cdot \rho_2)\rho_{4\nu} \cdot \rho_{1\mu} + g^{\mu\nu}(\rho_3 \cdot \rho_2)m^2 g_{\mu\nu} +$$

$$+ \rho^\nu_3 \cdot \rho^\mu_2 \cdot \rho_{4\mu} \cdot \rho_{1\nu} - g_{\mu\nu}\rho^\nu_3 \cdot \rho^\mu_2(\rho_4 \cdot \rho_1) + \rho_{4\nu} \cdot \rho_{1\mu}\rho^\nu_3 \cdot \rho^\mu_2 - m^2 \rho^\nu_3 \cdot \rho^\mu_2 g_{\mu\nu} -$$

$$- m^2 g^{\mu\nu} \cdot \rho_{4\mu} \cdot \rho_{1\nu} + m^2 g^{\mu\nu} g_{\mu\nu}(\rho_4 \cdot \rho_1) - m^2 g^{\mu\nu}\rho_{4\nu} \cdot \rho_{1\mu} + m^2 g^{\mu\nu} m^2 g_{\mu\nu}) =$$

$$= 16\frac{e^4}{t^2}((\rho_3 \cdot \rho_4)(\rho_2 \cdot \rho_1) - (\rho_3 \cdot \rho_2)(\rho_4 \cdot \rho_1) + (\rho_3 \cdot \rho_1)(\rho_2 \cdot \rho_4) - m^2(\rho_3 \cdot \rho_2) -$$

$$- (\rho_3 \cdot \rho_2)(\rho_4 \cdot \rho_1) + 4(\rho_3 \cdot \rho_2)(\rho_4 \cdot \rho_1) - (\rho_3 \cdot \rho_2)(\rho_4 \cdot \rho_1) + 4m^2(\rho_3 \cdot \rho_2) +$$

$$+ (\rho_3 \cdot \rho_1)(\rho_4 \cdot \rho_2) - (\rho_3 \cdot \rho_2)(\rho_4 \cdot \rho_1) + (\rho_3 \cdot \rho_4)(\rho_1 \cdot \rho_2) - m^2(\rho_3 \cdot \rho_2) -$$

$$- m^2(\rho_4 \cdot \rho_1) + 4m^2(\rho_4 \cdot \rho_1) - m^2(\rho_4 \cdot \rho_1) - 4m^4)$$

$$= 16\frac{e^4}{t^2}(2(\rho_3 \cdot \rho_4)(\rho_1 \cdot \rho_2) + (\rho_3 \cdot \rho_1)(\rho_4 \cdot \rho_2) - 2m^2(\rho_3 \cdot \rho_2) + 2m^2(\rho_1 \cdot \rho_4) - 4m^4) \xrightarrow{m=0}$$

$$= 16\frac{e^4}{t^2}(2(\rho_3 \cdot \rho_4)(\rho_1 \cdot \rho_2) + 2(\rho_3 \cdot \rho_1)(\rho_4 \cdot \rho_2))$$

Having considered p_1, p_2 as the incoming momenta and p_3, p_4, as the outcoming momenta, the mandlestam constants if we consider $m = 0$ are:

$$s = (p_1 + p_2)^2 = (p_3 + p_4)^2 = 2p_1 \cdot p_2 = 2p_3 \cdot p_4 \tag{3.1.6}$$

$$t = (p_1 - p_4)^2 = (p_3 - p_2)^2 = 2p_1 \cdot p_4 = 2p_2 \cdot p_3 \tag{3.1.7}$$

$$u = (p_1 - p_3)^2 = (p_4 - p_2)^2 = 2p_2 \cdot p_4 = 2p_1 \cdot p_3 \tag{3.1.8}$$

So, the matrix element is calculated:

$$\frac{1}{4}\sum_{s,s'} |\mathcal{M}_t|^2 = 8\frac{e^4}{t^2}(\frac{s^2 + u^2}{4}) = 2e^4\left(\left(\frac{s}{t}\right)^2 + \left(\frac{u}{t}\right)^2\right) \tag{3.1.9}$$

To find the s-channel matrix element, one can follow a detailed step-by-step procedure similar to that used

for the t-channel matrix element. Alternatively, by comparing the momentum indices of the t-channel matrix element to those of the s-channel matrix element, one can identify the necessary adjustments to transform the t-channel expression into the s-channel expression, and eventually simplify the calculation.

$$\sum_{s,s'} |\mathcal{M}_s|^2 = \frac{e^4}{q^4} \left([\bar{u}(p_2)\gamma^\mu v(p_1)][\bar{v}(p_4)\gamma_\mu u(p_3)]\right) \left([\bar{u}(p_2)\gamma^\mu v(p_1)][\bar{v}(p_4)\gamma_\mu u(p_3)]\right)^\dagger$$
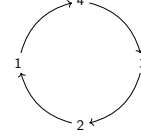
We observe that this is a cyclic permutation: $4 \to 3 \to 2 \to 1 \to 4$:

So, the result is going to be:

$$\sum_{s,s'} |\mathcal{M}_s|^2 = 16\frac{e^4}{s^2}(2(\rho_2 \cdot \rho_3)(\rho_4 \cdot \rho_1) + 2(\rho_2 \cdot \rho_4)(\rho_3 \cdot \rho_1))$$

And by using the same Mandlestam constants s, t and u, as before, we finally get:

$$\frac{1}{4}\sum_{s,s'} |\mathcal{M}_s|^2 = 8\frac{e^4}{s^2}(\frac{t^2 + u^2}{4}) = 2e^4\left(\left(\frac{t}{s}\right)^2 + \left(\frac{u}{s}\right)^2\right) \tag{3.1.10}$$

$$\sum_{s,s'} \bar{\mathcal{M}}_t \mathcal{M}_s = -\frac{e^4}{ts}\sum_{s,s'} \left([\bar{u}(p_3)\gamma^\mu u(p_2)][\bar{v}(p_4)\gamma_\mu v(p_1)]\right)^\dagger \left([\bar{u}(p_2)\gamma^\nu v(p_1)][\bar{v}(p_4)\gamma_\mu u(p_3)]\right)$$

$$= -\frac{e^4}{ts}\sum_{s,s'} \left([\bar{u}(p_2)\gamma^\mu u(p_3)][\bar{v}(p_1)\gamma_\mu v(p_4)]\right) \left([\bar{u}(p_2)\gamma^\nu v(p_1)][\bar{v}(p_4)\gamma_\mu u(p_3)]\right)$$

$$= -\frac{e^4}{ts}\sum_{s,s'} \left([\bar{u}(p_2)\gamma^\mu u(p_3)][\bar{u}(p_2)\gamma^\nu v(p_1)][\bar{v}(p_1)\gamma_\mu v(p_4)][\bar{v}(p_4)\gamma_\mu u(p_3)]\right) \xrightarrow{m=0}$$

$$= -\frac{e^4}{ts}tr[\not{p}_2\gamma^\mu\not{p}_3\gamma^\nu\not{p}_1\gamma_\mu\not{p}_4\gamma_\nu]$$

Because in helicity formalism $\not{p}$ and γ are 4x4 matrices we can use the trace identities to bring them in a form more convenient:

$$\sum_{s,s'} \bar{\mathcal{M}}_t \mathcal{M}_s = -\frac{e^4}{ts}tr[\not{p}_1\gamma^\nu\not{p}_2\gamma^\mu\not{p}_3\gamma_\nu\not{p}_4\gamma_\mu]$$

We will now use the identities:

- $\gamma^\nu\not{p} = p_\beta\gamma^\alpha\gamma^\beta(2p^\alpha - \not{p}\gamma^\alpha) = (2p^\alpha - \not{p}\gamma^\alpha)$

- $\not{p}\not{p} = p_\alpha p_\beta\gamma^\alpha\gamma^\beta = p^2 = 0$

By replacing: $p_4 = p_1 + p_2 - p_3$, we need to break the trace in 3 parts that we need to calculate separately:

$$\sum_{s,s'} \bar{\mathcal{M}}_t \mathcal{M}_s = -\frac{e^4}{ts}tr[\not{p}_1\gamma^\nu\not{p}_2\gamma^\mu\not{p}_3\gamma_\nu(\not{p}_1 + \not{p}_2 - \not{p}_3)\gamma_\mu]$$

$$= -\frac{e^4}{ts}\left(tr[\not{p}_1\gamma^\nu\not{p}_2\gamma^\mu\not{p}_3\gamma_\nu\not{p}_1\gamma_\mu] + tr[\not{p}_1\gamma^\nu\not{p}_2\gamma^\mu\not{p}_3\gamma_\nu\not{p}_2\gamma_\mu] - tr[\not{p}_1\gamma^\nu\not{p}_2\gamma^\mu\not{p}_3\gamma_\nu\not{p}_3\gamma_\mu]\right)$$

$$= -\frac{e^4}{ts}\left(T_{p_1} + T_{p_2} - T_{p_3}\right)$$

After calculations (the actual calculations are done by hand in the hand-written assignment) we have:

$$T_{p_2} = 0$$

$$T_{p_1} = -32(p_3 \cdot p_1)(p_2 \cdot p_1)$$

$$T_{p_3} = 32(p_2 \cdot p_3)(p_1 \cdot p_3)$$

We used permutation techniques to calculate easily the element T_{p_3} The final result for this matrix element, using the same Mandlestam constant s, t, u as before, is:

$$\frac{1}{4}\sum_{s,s'} \bar{\mathcal{M}}_t \mathcal{M}_s = -\frac{e^4}{4ts}\left(32(p_3 \cdot p_1)(p_2 \cdot p_1) - 32(p_2 \cdot p_3)(p_1 \cdot p_3)\right)$$

$$= -\frac{e^4}{4ts}\left(32\frac{-us}{4} - 32\frac{ut}{4}\right) = 2e^4\left(\frac{u}{t} + \frac{u}{s}\right)$$

Similarly, we calculate the final element:

$$\frac{1}{4}\sum_{s,s'} \bar{\mathcal{M}}_s \mathcal{M}_t = -\frac{e^4}{4ts}\left(32(p_4 \cdot p_2)(p_2 \cdot p_1) - 32(p_1 \cdot p_4)(p_2 \cdot p_4)\right)$$

$$= -\frac{e^4}{4ts}\left(32\frac{-us}{4} - 32\frac{ut}{4}\right) = 2e^4\left(\frac{u}{t} + \frac{u}{s}\right)$$

Eventually, the spin-averaged matrix element is:

$$\langle|\mathcal{M}|^2\rangle = 2e^4\left(\left(\frac{u}{t} + \frac{u}{s}\right) + \left(\frac{u}{t} + \frac{u}{s}\right) + \left(\frac{t}{s}\right)^2 + \left(\frac{u}{s}\right)^2 + \left(\frac{s}{t}\right)^2 + \left(\frac{u}{t}\right)^2\right)$$

$$= 2e^4\left(2\frac{u(s+t)}{ts} + \left(\frac{t}{s}\right)^2 + \left(\frac{u}{s}\right)^2 + \left(\frac{s}{t}\right)^2 + \left(\frac{u}{t}\right)^2\right)$$

$$= 2e^4\left(2\frac{u^2}{ts} + \left(\frac{t}{s}\right)^2 + \left(\frac{u}{s}\right)^2 + \left(\frac{s}{t}\right)^2 + \left(\frac{u}{t}\right)^2\right)$$

$$= 2e^4\left(u^2\left(\frac{1}{t^2} + 2\frac{1}{ts} + \frac{1}{s^2}\right) + \left(\frac{t}{s}\right)^2 + \left(\frac{s}{t}\right)^2\right)$$

$$\langle|\mathcal{M}|^2\rangle = 2e^4\left(u^2\left(\frac{1}{t} + \frac{1}{s}\right)^2 + \left(\frac{t}{s}\right)^2 + \left(\frac{s}{t}\right)^2\right) \tag{3.1.11}$$

3.2 QCD: elementary processes

3.2.1 Study the elementary process $u\bar{u} \to u\bar{u}$ analogous to Bhabha scattering in QED

The process of calculating scattering amplitudes and cross-sections has been analyzed in the previous subsection. The steps to calculate cross sections for jet production in hadronic collisions are exactly the same for QCD as it is in QED. However, in QCD it is essential not only to sum over all possible reactions of quarks, antiquarks and gluons, but also to sum over all final and initial colors, since we are in $SU(3)$ group.
Let us remind the cross section for the Bhabha scattering process 3.1.11:

$$\langle|\mathcal{M}|^2\rangle = 2e^4 \left(u^2 \left(\frac{1}{t} + \frac{1}{s} \right)^2 + \left(\frac{t}{s} \right)^2 + \left(\frac{s}{t} \right)^2 \right)$$

In order to calculate the $u\bar{u} \to u\bar{u}$ cross section, we simply replace the e^2 QED coupling by g^2 times an $SU(3)$ factor for the color summation. This specific process is more easily analyzed using helicity formalism, than using the spin summation technique. The second one is rather difficult as each term receives different color factors so the calculations will be exhausting.

(a) scattering: t-channel

(b) annihilation: s-channel

In order to calculate the total scattering amplitude, we have to distinguish the 3 cases and sum over colors for each case differently.

s - channel

We first express the scattering amplitude of the s-channel diagram.

$$
\begin{aligned}
\mathcal{M}_s &= \bar{v}(p_2)(-ig_s\gamma^\mu T^a_{i_1,i_2})u(p_1) \left(-\delta_{ab}\frac{g_{\mu\nu}}{q^2} \right) u(p_4)(-ig_s\gamma^\nu T^b_{i_4,i_3})\bar{v}(p_3) \\
&= (-ig_s)^2 \bar{v}(p_2)\gamma^\mu T^a_{i_1,i_2}u(p_1) \left(-\frac{1}{s^2} \right) u(p_4)\gamma_\mu T^a_{i_4,i_3}\bar{v}(p_3) \\
&= \frac{g_s^2}{s^2} T^a_{i_1,i_2} T^a_{i_4,i_3} \bar{v}(p_2)\gamma^\mu u(p_1)u(p_4)\gamma_\mu \bar{v}(p_3)
\end{aligned}
\tag{3.2.1}
$$

The operation is similar to Bhabha scattering, this means that the scattering amplitudes in the end will be exactly the same, plus an extra term that stems from the color summation which is an independent operation.

$$|\mathcal{M}_s|^2 = \left(\text{} \right) \times \left(\text{} \right)^\dagger$$

We sum over initial and final colors and spins:

$$\frac{1}{4}\sum_{s,s'}|\mathcal{M}_s|^2 = \frac{g_s^2}{4s^2}\sum_{s,s'}\sum_{\text{colors}} T^a_{i_1,i_2}T^a_{i_4,i_3}\bar{v}(p_2)\gamma^\mu u(p_1)u(p_4)\gamma_\mu\bar{v}(p_3)\times\left(T^b_{i_1,i_2}T^b_{i_4,i_3}\bar{v}(p_2)\gamma^\mu u(p_1)u(p_4)\gamma_\mu\bar{v}(p_3)\right)^\dagger$$

$$= \frac{g_s^2}{4s^2}\sum_{s,s'}\sum_{\text{colors}} T^a_{i_1,i_2}T^a_{i_4,i_3}\bar{v}(p_2)\gamma^\mu u(p_1)u(p_4)\gamma_\mu\bar{v}(p_3)\times T^b_{i_2,i_1}T^b_{i_3,i_4}\bar{u}(p_1)\gamma^\nu v(p_2)v(p_3)\gamma_\nu\bar{u}(p_4)$$

$$= \frac{g_s^2}{4s^2}\sum_{s,s'}[\bar{v}(p_2)\gamma^\mu u(p_1)\bar{u}(p_1)\gamma^\nu v(p_2)][u(p_4)\gamma_\mu\bar{v}(p_3)v(p_3)\gamma_\nu\bar{u}(p_4)]\sum_{\text{colors}}[T^a_{i_1,i_2}T^b_{i_2,i_1}][T^a_{i_4,i_3}T^b_{i_3,i_4}]$$

$$\overset{m=0}{=} \frac{g_s^2}{4s^2}\left(tr[\not{p}_2\gamma^\mu\not{p}_1\gamma^\nu]\times tr[\not{p}_4\gamma_\mu\not{p}_3\gamma_\nu]\right)\frac{1}{3}\frac{1}{3}\left(tr[T^aT^b]\right)^2$$

We have already calculated for Bhabha scattering:

$$tr[\not{p}_3\gamma^\mu\not{p}_2\gamma^\nu]tr[\not{p}_4\gamma_\mu\not{p}_1\gamma_\nu] = 32\left((p_3\cdot p_4)(p_2\cdot p_1)+(p_3\cdot p_1)(p_2\cdot p_4)\right) \tag{3.2.2}$$

By a permutation $1\to 3\to 2\to 1$, we find:

$$\frac{1}{4}\sum_{s,s'}|\mathcal{M}_s|^2 = 32\frac{g_s^2}{4s^2}\left((p_2\cdot p_4)(p_1\cdot p_3)+(p_2\cdot p_3)(p_1\cdot p_4)\right)\frac{1}{9}\left(tr[T^aT^b]\right)^2$$

$$\overset{\text{replace } s,t,u}{=} 8\frac{g_s^2}{4s^2}\left(u^2+t^2\right)\frac{1}{9}\left(tr[T^aT^b]\right)^2$$

For the color decomposition we can use the identity:

$$\frac{1}{9}(tr[T^aT^b])^2 = \frac{1}{9}T_R^2\delta^{ab}\delta^{ab} = \frac{1}{4\cdot 9}8 = \frac{2}{9} \tag{3.2.3}$$

Eventually, the s-channel term is:

$$\frac{1}{4}\sum_{s,s'}|\mathcal{M}_s|^2 = \frac{4}{9}\frac{g_s^2}{s^2}\left(u^2+t^2\right) \tag{3.2.4}$$

t - channel

Using the same logic we calculate the t-channel matrix element. The expression for the scattering amplitude of the t-channel diagram is:

$$\mathcal{M}_t = \bar{v}(p_3)(-ig_s\gamma^\nu T^b_{i_1,i_3})\bar{v}(p_2)\left(-\delta_{ab}\frac{g_{\mu\nu}}{q^2}\right)u(p_4)(-ig_s\gamma^\mu T^a_{i_4,i_2})u(p_1)$$

$$= \frac{g_s^2}{t^2}T^a_{i_1,i_3}T^a_{i_4,i_2}\bar{v}(p_3)\gamma_\mu\bar{v}(p_2)u(p_4)\gamma^\mu u(p_1) \tag{3.2.5}$$

$$\frac{1}{4}\sum_{s,s'}|\mathcal{M}_t|^2 = \frac{g_s^2}{4t^2}\sum_{s,s'}\sum_{\text{colors}} T^a_{i_1,i_3}T^a_{i_4,i_2}\bar{v}(p_3)\gamma_\mu\bar{v}(p_2)u(p_4)\gamma^\mu u(p_1)) \times \left(T^b_{i_1,i_3}T^b_{i_4,i_2}\bar{v}(p_2)\gamma_\nu\bar{v}(p_3)u(p_4)\gamma^\nu u(p_1)\right)^\dagger$$

$$= \frac{g_s^2}{4t^2}\sum_{s,s'}[u(p_4)\gamma^\mu u(p_1)\bar{u}(p_1)\gamma^\nu\bar{u}(p_4)][\bar{v}(p_3)\gamma_\mu\bar{v}(p_2)v(p_2)\gamma_\nu v(p_3)]\sum_{\text{colors}} T^a_{i_1,i_3}T^b_{i_3,i_1}T^a_{i_4,i_2}T^b_{i_2,i_4}$$

$$= \frac{g_s^2}{4t^2}tr[\not{p}_4\gamma^\mu\not{p}_1\gamma^\nu]tr[\not{p}_3\gamma_\mu\not{p}_2\gamma_\nu]\frac{1}{9}\left(tr[T^aT^b]\right)^2$$

Again, using the relation 3.2.2 for the trace calculation, and 3.2.3 for the color decomposition, the equation becomes:

$$\frac{1}{4}\sum_{s,s'}|\mathcal{M}_t|^2 = 32\frac{g_s^2}{4t^2}\left((p_3\cdot p_4)(p_2\cdot p_1)+(p_3\cdot p_1)(p_2\cdot p_4)\right)\frac{1}{9}\left(tr[T^aT^b]\right)^2$$

$$\overset{\text{replace } s,t,u}{=} 32\frac{g_s^2}{4t^2}\left(\frac{s^2+u^2}{4}\right)\frac{2}{9}$$

$$\frac{1}{4}\sum_{s,s'}|\mathcal{M}_t|^2 = \frac{4}{9}\frac{g_s^2}{t^2}\left(s^2+u^2\right) \tag{3.2.6}$$

Combined terms $\mathcal{M}_t\bar{\mathcal{M}}_s$, $\bar{\mathcal{M}}_t\mathcal{M}_s$

We only need to calculate the first term $\mathcal{M}_t\bar{\mathcal{M}}_s$, since the second term is identical.

$$\frac{1}{4}\sum_{s,s'}\mathcal{M}_t\bar{\mathcal{M}}_s = \frac{g_s^2}{4ts}\sum_{s,s'}\sum_{colors} T^a_{i_1,i_3}T^a_{i_4,i_2}T^b_{i_2,i_1}T^b_{i_3,i_4}\left[\bar{v}(p_2)\gamma_\mu\bar{v}(p_3)u(p_4)\gamma^\mu u(p_1)\right]\left[\bar{u}(p_1)\gamma^\nu v(p_2)v(p_3)\gamma_\nu\bar{u}(p_4)\right]$$

$$= \frac{g_s^2}{4ts}\sum_{colors}\left(T^a_{i_1,i_3}T^b_{i_3,i_4}\right)\left(T^a_{i_4,i_2}T^b_{i_2,i_1}\right)\sum_{s,s'}\left[\bar{v}(p_2)\gamma_\mu\bar{v}(p_3)v(p_3)\gamma_\nu\bar{u}(p_4)u(p_4)\gamma^\mu u(p_1)\bar{u}(p_1)\gamma^\nu v(p_2)\right]$$

$$\overset{\text{m=0}}{=} \frac{g_s^2}{4ts}\frac{1}{9}tr[T^aT^bT^aT^b]tr[\not{p}_2\gamma_\mu\not{p}_3\gamma_\nu\not{p}_4\gamma^\mu\not{p}_1\gamma^\nu]$$

Each trace will be calculated separately using previous results or equations from theory:

- Spin summation using the calculations from Bhabha scattering:

$$tr[\not{p}_2\gamma_\mu\not{p}_3\gamma_\nu\not{p}_4\gamma^\mu\not{p}_1\gamma^\nu] = tr[\not{p}_4\gamma^\mu\not{p}_1\gamma^\nu\not{p}_2\gamma_\mu\not{p}_3\gamma_\nu] = tr[\not{p}_1\gamma^\nu\not{p}_4\gamma^\mu\not{p}_3\gamma_\nu\not{p}_2\gamma_\mu]$$

$$= 32\left((p_4\cdot p_3)(p_1\cdot p_3)-(p_1\cdot p_3)(p_4\cdot p_1)\right) = 32\left(\frac{su}{4}+\frac{ut}{4}\right) = 8\left(su+ut\right) \tag{3.2.7}$$

- Color summation, using equations from Peskin:

$$\frac{1}{9}tr[T^a T^b T^a T^b] = \frac{1}{9}\left[\underbrace{C_2(r)}_{\frac{4}{3}} - \frac{1}{2}\underbrace{N_c}_{3}\right]\underbrace{tr[T^a]}_{4} = -\frac{2}{27} \tag{3.2.8}$$

So eventually, the term is found:

$$\frac{1}{4}\sum_{s,s'}\mathcal{M}_t\bar{\mathcal{M}}_s = \frac{g_s^2}{4ts}\left(-\frac{2}{27}\right)8\left(su+ut\right) = -\frac{4}{27}\frac{g_s^2}{ts}\left(su+ut\right) = \frac{1}{4}\sum_{s,s'}\bar{\mathcal{M}}_t\mathcal{M}_s \tag{3.2.9}$$

Now, combining 3.2.4, 3.2.6 and 3.2.9 we can calculate the total scattering amplitude:

$$\langle|\mathcal{M}|^2\rangle = \frac{4}{9}\frac{g_s^2}{s^2}\left(u^2+t^2\right) + \frac{4}{9}\frac{g_s^2}{t^2}\left(u^2+s^2\right) - 2\cdot\frac{4}{27}\frac{g_s^2}{ts}(su+ut)$$

$$= \frac{4g_s^2}{9}\left(\frac{u^2}{t^2} + \frac{s^2}{t^2} + \frac{u^2}{s^2} + \frac{t^2}{s^2} - \frac{2}{3}\frac{u(s+t)}{st}\right)$$

$$= \frac{4g_s^2}{9}\left(\frac{u^2}{t^2} + \frac{s^2}{t^2} + \frac{u^2}{s^2} + \frac{t^2}{s^2} - \frac{2}{3}\frac{u(s+t)}{st}\right)$$

$$\langle|\mathcal{M}|^2\rangle = \frac{4g_s^2}{9}\left(\frac{u^2+s^2}{t^2} + \frac{u^2+t^2}{s^2} - \frac{2}{3}\frac{u^2}{st}\right) \tag{3.2.10}$$

Comparing the result from 3.2.10 to the one in Bhabha scattering 3.1.11, we observe that there is an extra term in the parenthesis which stems from the color summation.

4 Applications to HELAC-PEGAS

4.1 HELAC-PHEGAS program

In the first phase, HELAC builds the instructions of the recursive (Dyson-Schwinger) calculation of the scattering amplitude for an arbitrary input process. These instructions are known as the skeleton of the calculation. The second phase involves numerical evaluation of the amplitudes and integration over phase space. Integration is performed using the programs PHEGAS[6] and KALEU[7]. In our case, KALEU phase space generator is selected. A brief overview of the Dyson-Schwinger recursive algorithm will be presented, as it is the main component refined during this project.

HELAC is a FORTRAN based package that uses the Dyson-Schwinger recursive algorithm to compute helicity amplitudes for arbitrary scattering processes. The computational cost of this algorithm, that is the steps to solve the recursive equations grows asymptotically as 3^n in contrast to Feynman diagrams approach which grows as $n!$, where n is the number of particles involved in the process. The Dyson-Schwinger equations express recursively the n-point Green functions in terms of 1-,2-,...,(n-1)-point functions.

Before presenting the recursive equations, we need to write down the appropriate definitions.[8] Let P be the sum of all the external momenta of the particles involved in the process $P = \sum_{i\in I}p_i$ where $I\subset 1,...,n$. The sub-amplitude of a vector field is:

$$b_\mu(P) = \quad\text{〜〜}\bigcirc$$

Accordingly, for a fermion current and an antifermion with momentum P we note:

$$\psi_\mu(P) = \quad\text{——◀}\bigcirc$$

$$\bar{\psi}_\mu(P) = \quad\text{——▶}\bigcirc$$

To provide an example, let us consider a QED process where we calculate the output boson in a two particle interaction:

$$b_\mu(P) = \sum_{i=1}^{n} \delta_{P=p_i} b_\mu(p_i) + \sum_{P=P_1+P_2} (ig)\ \Pi_\nu^\mu\ \bar{\psi}(P_2)\gamma^\nu\psi(P_1)\epsilon(P_1,P_2)$$

Where $\Pi_\nu^\mu = \frac{i}{P^2-m^2}\left(-g_\nu^\mu + \frac{P^\mu P_\nu}{P^2-\xi\mu^2}(1-\xi)\right)$ the propagator.

For the fermion with momentum P:

$$\psi_\mu(P) = \sum_{i=1}^{n} \delta_{P=p_i} \psi_\mu(p_i) + \sum_{P=P_1+P_2} (ig)\ P\ \slashed{b}(P_2)\psi(P_1)\epsilon(P_1,P_2)$$

Where $P = \frac{i}{\slashed{P}-m}$.

Finally, for the antifermion:

$$\psi_\mu(P) = \sum_{i=1}^{n} \delta_{P=p_i} \psi_\mu(p_i) + \sum_{P=P_1+P_2} (ig)\ \bar{\psi}(P_1)\slashed{b}(P_2)\ \bar{P}\ \epsilon(P_1,P_2)$$

Where $\bar{P} = \frac{i}{-\slashed{P}-m}$. This type of current computation is useful especially for the first project of the internship. For QCD processes, it is essential that color be taken into consideration; therefore, the calculations follow the same logic but also involve a summation over color degrees.

4.2 1st Project: Explicit calculations of currents in the context of SMEFT

In this project, I will only present the results of the dimension-6 O_{uH} operator analytically, as they were calculated explicitly using the python library that has been developed as a part of the project. The rest of the operators calculated have more complicated and larger in length currents, so they will only be provided on the GitHub repository[9].

The currents are computed in both Lorentz and lightcone representations. For each current, we also provide the formula obtained when the propagator (more precisely its numerator) of the outgoing particle is attached. In the lightcone representation, which is used for simplification - to keep a more compact form of the vector components, a 4-vector $V^\mu = (V^1, V^2, V^3, V^4)$ is expressed as $V^\mu = (V^1 + V^4, V^1 - V^4, V^2 + iV^3, V^2 - iV^3)$. The metric signature used is (-,+,+,+).

$\underline{O_{uH}}$ Starting with the simplest O_{uH} operator for the vertex $t\bar{t}H$, we will examine 3 possible scenarios depending on the ingoing and outgoing particles: fermion, antifermion or Higgs as outgoing particles.

$$t\bar{t}H = \qquad\qquad : \quad O_{uH} = \frac{iv^2}{\sqrt{2}}(P_L C^{u\phi*}_{f_2 f_1} + P_R C^{u\phi}_{f_1 f_2})$$

The symbols $\psi_{1\mu}$, $\psi_{2\mu}$ where $\mu = 0, 1, ..., 3$, represent the fermion and antifermion respectively.

- For the vertex $t + \bar{t} \to H$ the current was calculated and cross checked.
  Lorentz representation:

$$\frac{\sqrt{2}iC^{u\phi}v^2}{2}\left[g_L\psi_{13}\psi_{23} + g_L\psi_{14}\psi_{24} + g_R\psi_{11}\psi_{21} + g_R\psi_{12}\psi_{22}\right]$$

  Lightcone representation:

$$\left[\frac{\sqrt{2}iC^{u\phi}v^2 g_R\psi_{11}\psi_{21}}{2}\right]$$

- For the vertex $t + H \to \bar{t}$ the current was calculated and cross checked:
  Lorentz representation with propagator considered:

$$\frac{\sqrt{2}iC^{u\phi}bv^2}{2}\begin{bmatrix} -g_L\psi_{13}(P_0 + P_3) - g_L\psi_{14}(P_1 - iP_2) + g_R m\psi_{11} \\ -g_L\psi_{13}(P_1 + iP_2) - g_L\psi_{14}(P_0 - P_3) + g_R m\psi_{12} \\ g_L m\psi_{13} - g_R\psi_{11}(P_0 - P_3) + g_R\psi_{12}(P_1 - iP_2) \\ g_L m\psi_{14} + g_R\psi_{11}(P_1 + iP_2) - g_R\psi_{12}(P_0 + P_3) \end{bmatrix}$$

  Lightcone representation with propagator considered:

$$\frac{\sqrt{2}iC^{u\phi}bv^2}{2}\begin{bmatrix} -P_0 g_L\psi_{13} - P_3 g_L\psi_{14} + g_R m\psi_{11} \\ -P_1 g_L\psi_{14} - P_2 g_L\psi_{13} + g_R m\psi_{12} \\ -P_1 g_R\psi_{11} + P_3 g_R\psi_{12} + g_L m\psi_{13} \\ -P_0 g_R\psi_{12} + P_2 g_R\psi_{11} + g_L m\psi_{14} \end{bmatrix}$$

Lightcone representation without propagator considered:

$$\frac{\sqrt{2}iC^{u\phi}bv^2}{2}\begin{bmatrix} g_R\psi_{11} \\ g_R\psi_{12} \\ g_L\psi_{13} \\ g_L\psi_{14} \end{bmatrix}$$

- For the vertex $\bar{t} + H \rightarrow t$ the current was calculated and cross checked:

  Lorentz representation with propagator considered:

$$\frac{\sqrt{2}iC^{u\phi}bv^2}{2}\begin{bmatrix} g_L\psi_{23}(P_0 - P_3) - g_L\psi_{24}(P_1 + iP_2) + g_Rm\psi_{21} \\ -g_L\psi_{23}(P_1 - iP_2) + g_L\psi_{24}(P_0 + P_3) + g_Rm\psi_{22} \\ g_Lm\psi_{23} + g_R\psi_{21}(P_0 + P_3) + g_R\psi_{22}(P_1 + iP_2) \\ g_Lm\psi_{24} + g_R\psi_{21}(P_1 - iP_2) + g_R\psi_{22}(P_0 - P_3) \end{bmatrix}$$

  Lightcone representation with propagator considered:

$$\frac{\sqrt{2}iC^{u\phi}bv^2}{2}\begin{bmatrix} P_1 g_L\psi_{23} - P_2 g_L\psi_{24} + g_Rm\psi_{21} \\ P_0 g_L\psi_{24} - P_3 g_L\psi_{23} + g_Rm\psi_{22} \\ P_0 g_R\psi_{21} + P_2 g_R\psi_{22} + g_Lm\psi_{23} \\ P_1 g_R\psi_{22} + P_3 g_R\psi_{21} + g_Lm\psi_{24} \end{bmatrix}$$

Lightcone representation without propagator considered:

$$\frac{\sqrt{2}iC^{u\phi}bv^2}{2}\begin{bmatrix} g_R\psi_{21} \\ g_R\psi_{22} \\ g_L\psi_{23} \\ g_L\psi_{24} \end{bmatrix}$$

The same pattern is used for the rest of the SMEFT vertices. All results are presented in detail, in the same way as above in the GitHub repository[9].

On GitHub[9], you can find all the necessary Python scripts to perform symbolic calculations with spinors and other mathematical objects such as metrics, vectors and Lorentz and light-cone representations. Inside the SMEFT folder, one can spot the SMEFT_main.ipynb jupyter notebook file, which illustrates the results of the three SMEFT operators acting on spinors vectors or scalars depending on the situation. This file is using the standard_formulas.py, python library that includes all the standard objects to build our framework, such as the metric, the helicities or the polarizations. One level up from there, the SMEFT_library.py, includes all the necessary functions to calculate the output of the SMEFT operators acting on spinors, vectors or scalars. The calculations and results of the output currents inside the SMEFT_main.ipynb file are quite clear and useful for the next step, which is the implementation in HELAC to generate recursive amplitude calculations.

4.3 2^d Project: a LO study of top-philic Z' production in HELAC

In this project, a Z' boson implementation is integrated into the HELAC source code. According to the study by [2], the Z' boson is a color singlet, and its interaction with fermionic currents is described by the Lagrangian:

$$L_{int} = \bar{t}\gamma_\mu(c_L P_L + c_R P_R)tZ^{\mu'} = c_t\bar{t}\gamma_\mu(cos(\theta)P_L + sin(\theta)P_R)tZ^{\mu'} \tag{4.3.1}$$

Where $P_{L/R} = (1 \pm \gamma^5)/2$, $c_t = \sqrt{c_L^2 + c_R^2}$ and $\tan\theta = \frac{C_R}{C_L}$ the projection operators. The decay width of Z' to a top-antitop pair is given by:

$$\Gamma(Z' \to t\bar{t}) = \frac{c_t^2 M_{Z'}}{8\pi}\sqrt{1 - \frac{4m_t^2}{M_{Z'}^2}} \times \left[1 - \frac{m_t^2}{M_{Z'}^2}\left(1 - 3sin(2\theta)\right)\right]^{\theta=\frac{\pi}{2}} \stackrel{}{=} 229.74 \text{ (GeV)} \tag{4.3.2}$$

Based on the paper[2], the largest contribution at the LHC comes from the four-top quark final state. Specifically, the strong four-top production has been shown to be independent of the angle θ, therefore in order to study the tree-level top production with Z'-strahlung, we may use the simplification $\theta = \frac{\pi}{2}$.

We have implemented the Z' boson in the HELAC-PHEGAS and made a simple phenomenological study in the context of four-top production at LHC in $pp \to t\bar{t}t\bar{t}$ interactions at LO in perturbation theory.

In HELAC interface, in order to avoid the large computational cost in a $pp \to t\bar{t}t\bar{t}$ process, instead of summing over all possible incoming partons (p=u,d,s,c,b), we push all the contributions in a single generation (using only $u\bar{u}$ in our case). Since QCD is flavor blind-the coupling is independent of the flavor- and since we consider massless light quarks at $O(\alpha_s^4)$ all processes of the previous form share the same amplitude. In this way, only the three subprocesses: $u\bar{u} \to t\bar{t}t\bar{t}$, $\bar{u}u \to t\bar{t}t\bar{t}$ and $gg \to t\bar{t}t\bar{t}$ are computed in practice, where the first two once incorporate contributions from u,d,c,s,b quarks in the initial state. In total, for the $O(\alpha_s^4)$-not the full LO, 22 Feynman diagrams were registered for the first two cases, while 120 for the last case, which constitutes the main channel of the process. A comparison of the cross sections of the processes, in both the SM and the SM with Z' boson, is presented in the table 1. Roughly a 10% increase is denoted for the secondary channels, while the main channel shows a significant 70% after the implementation of the resonance in the model.

Models in $O(\alpha_s^4)$	$p\bar{p} \to t\bar{t}t\bar{t}$ ($\times 10^{-6}$ **pb**)	$\bar{p}p \to t\bar{t}t\bar{t}$ ($\times 10^{-6}$ **pb**)	$gg \to t\bar{t}t\bar{t}$ ($\times 10^{-5}$ **pb**)
SM	431 ± 1	432 ± 1	743 ± 1
SM $+Z'$	472 ± 1	471 ± 2	1282 ± 2

Table 1: Comparison of cross sections (**pb**) for processes in the Standard Model (SM) and the SM extended with a Z' boson at coliision energy $\sqrt{s} = 13$ TeV. The errors presented are the Monte-Carlo uncertainties.

Phase space generation was carried out for two different collision energies, 13 TeV and 14 TeV. In this simulation, we assumed a parameter value of $c_t = 2$, a top quark mass of $m_t = 173.0$ [GeV], and utilized the LHAPDF dataset NNPDF3.1[10] (no overall renormalization). The transverse momentum p_T and pseudorapidity η distributions were plotted for the top quarks associated to the resonant Z' decay. The results are qualitatively similar to those in the paper, especially in the case of 14 TeV collision energy. On the paper[2], a more rigorous study of the four top production takes place at NLO accuracy, with realistic final states arising from top-quark decays and considering kinematical cuts. Our project instead focuses on the simpler case of fully inclusive four top production at LO for QCD. Furthermore, we repeated the simulation in the context of the SM in order to make comparisons. First the simple case of the SM at 13 TeV, without Z'

resonance is presented in the figure below. In figure 10, the same distributions are reproduced for collision energy equal to 14 TeV.
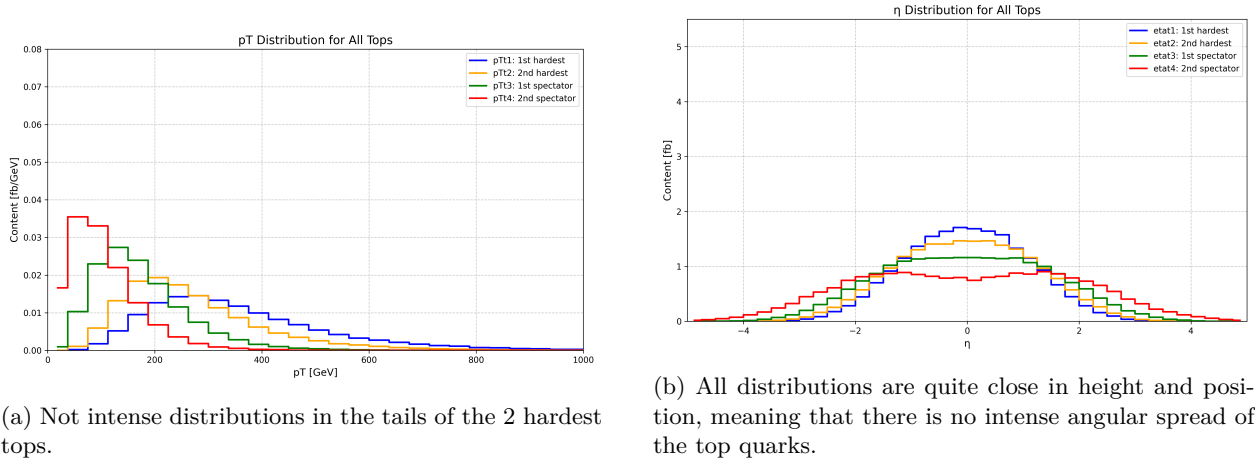

(a) Not intense distributions in the tails of the 2 hardest tops.

(b) All distributions are quite close in height and position, meaning that there is no intense angular spread of the top quarks.

Figure 8: $\sqrt{s} = 13$ TeV, $pp \to t\bar{t}t\bar{t}$-Standard Model.

(a) A slight plateau formed in the region 500-800 [GeV].

(b) More intense peaks compared to the SM.
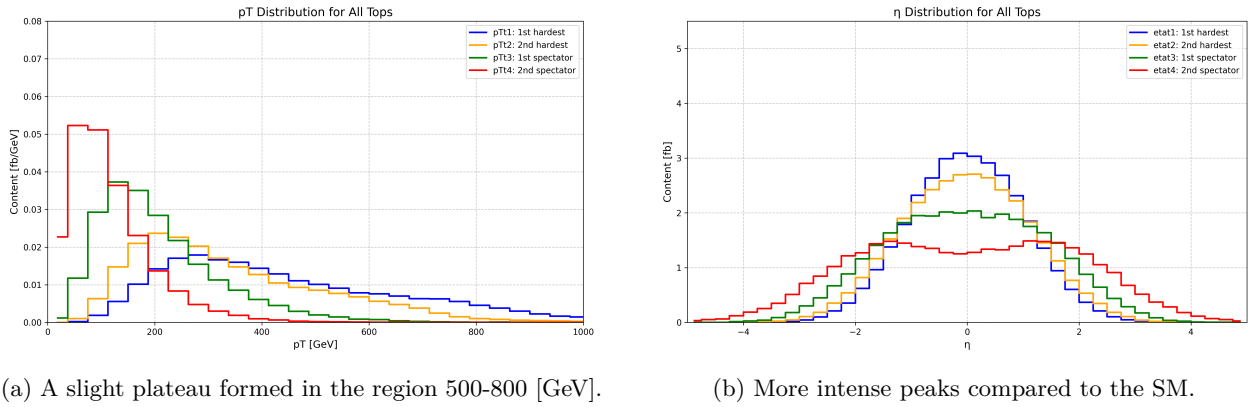
Figure 9: $\sqrt{s} = 13$ TeV, $pp \to t\bar{t}t\bar{t}$-through Z' decay.

(a) For the 1st harders top the plateau is more intense approaching the first peak in height. The second hardest top also exhibits such increase in the distribution.

(b) Wider distribution meaning broad angular distribution due to the contribution of the Z' decay.

Figure 10: $\sqrt{s} = 14$ TeV, $pp \to t\bar{t}t\bar{t}$-through Z' decay.

Comparing the figures 8 and 9, it is obvious that the distributions of the transverse momenta and pseudo-rapidities are intensified in the Z' case. Specifically, a slight p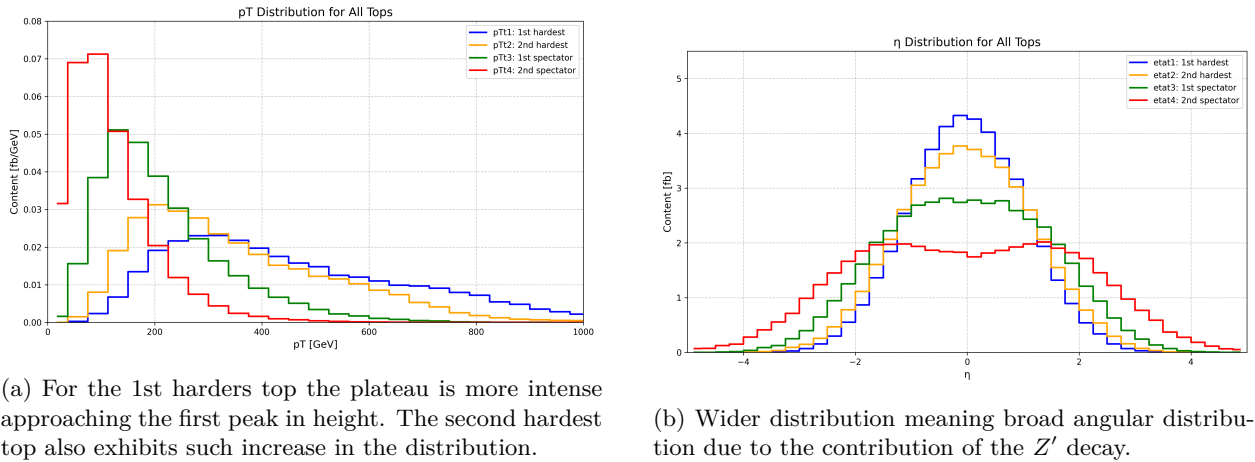lateau is formed for the transverse momentum of the hardest top at $p_T > 500$ [GeV]. Regarding the position of the peaks in the p_T diagrams, the peaks of all top quarks are closely concentrated in a region below 300 [GeV], particularly for the SM case. However, in the resonance cases, all the new physics seems to be created in the region above 300 [GeV] where the distributions of the 1st and 2nd hardest top seem to rise. This enhancement, first noted in Figure 9, becomes even more pronounced in Figure 10, where the collision energy is increased to 14 TeV. Therefore, higher energies not only increase the possibility of clear identification of this resonance, but also raise the possibility of discovering new physics phenomena in general.

As mentioned in the paper, the distribution is expected to exhibit a peak shift to the point $\frac{M_{Z'}}{2} \approx 750$ [GeV]. This expectation is somewhat reflected in our results, as a subtle bump begins to form in this region.

References

[1] J. Ellis, M. Madigan, K. Mimasu, V. Sanz, and T. You, "Top, Higgs, Diboson and Electroweak Fit to the Standard Model Effective Field Theory," *JHEP*, vol. 04, p. 279, 2021. [Online]. Available: https://inspirehep.net/literature/1835103

[2] J. H. Kim, K. Kong, S. J. Lee, and G. Mohlabeng, "Probing TeV scale Top-Philic Resonances with Boosted Top-Tagging at the High Luminosity LHC," *Phys. Rev. D*, vol. 94, no. 3, p. 035023, 2016. [Online]. Available: https://inspirehep.net/literature/1452565

[3] C. G. Papadopoulos and M. Worek, "Multi-parton cross sections at hadron colliders," *Eur. Phys. J. C*, vol. 50, pp. 843–856, 2007. [Online]. Available: https://inspirehep.net/literature/700223

[4] S. Dawson, "Introduction to smeft," https://indico.cern.ch/event/1131319/contributions/4895936/attachments/2479748/4256628/cteq_2022_dawson.pdf, 2022, accessed: August 19, 2024.

[5] F. Maltoni, E. Vryonidou, and C. Zhang, "Higgs production in association with a top-antitop pair in the Standard Model Effective Field Theory at NLO in QCD," *JHEP*, vol. 10, p. 123, 2016. [Online]. Available: https://inspirehep.net/literature/1477023

[6] A. Cafarella, C. G. Papadopoulos, and M. Worek, "Helac-Phegas: A Generator for all parton level processes," pp. 1941–1955, 2009. [Online]. Available: https://inspirehep.net/literature/764008

[7] A. van Hameren, "Kaleu: A General-Purpose Parton-Level Phase Space Generator," 3 2010. [Online]. Available: https://helac-phegas.web.cern.ch/kaleu.html

[8] A. Kanaki and C. G. Papadopoulos, "HELAC: A Package to compute electroweak helicity amplitudes," pp. 306–315, 2000. [Online]. Available: https://inspirehep.net/literature/523745

[9] G. Zachou, "Qft numerical calculations," https://github.com/GeorgiaZ9/QFT_numerical_calculations/tree/main, 2024, accessed: August 24, 2024.

[10] R. D. Ball *et al.*, "Parton distributions from high-precision collider data," *Eur. Phys. J. C*, vol. 77, no. 10, p. 663, 2017. [Online]. Available: https://inspirehep.net/literature/1602475